applied optics

Nonlinear diffusion model for annealed proton-exchanged waveguides in zirconium-doped lithium niobate

Carsten Langrock,[1,*] Rostislav V. Roussev,[2] Giovanni Nava,[3,4] Paolo Minzioni,[4] Nicola Argiolas,[5] Cinzia Sada,[5] and Martin M. Fejer[1]

[1]Edward L. Ginzton Laboratory, Stanford University, 348 Via Pueblo Mall, Stanford, California 94305, USA
[2]Science and Technology Division, Corning Incorporated, Corning, New York 14831, USA
[3]Department of Medical Biotechnology and Translational Medicine, University of Milan, Via Fratelli Cervi 93, I-20090 Milan, Italy
[4]Department of Electrical, Computer and Biomedical Engineering and CNISM, University of Pavia, Via Ferrata 5A, 27100 Pavia, Italy
[5]Department of Physics and CNISM, University of Padova, Via Marzolo 8, 35131 Padova, Italy
*Corresponding author: langrock@stanford.edu

Received 21 April 2016; revised 10 June 2016; accepted 26 July 2016; posted 26 July 2016 (Doc. ID 263625); published 11 August 2016

Photorefractive-damage- (PRD) resistant zirconium-oxide-doped lithium niobate is investigated as a substrate for the realization of annealed proton-exchanged (APE) waveguides. Its advantages are a favorable distribution coefficient, PRD resistance comparable to magnesium-oxide-doped lithium niobate, and a proton-diffusion behavior resembling congruent lithium niobate. A 1D model for APE waveguides was developed based on a previous model for congruently melting lithium niobate. Evidence for a nonlinear index dependence on concentration was found.

OCIS codes: (160.4330) Nonlinear optical materials; (160.3730) Lithium niobate; (190.0190) Nonlinear optics; (130.2790) Guided waves; (130.2260) Ferroelectrics; (130.7405) Wavelength conversion devices.

http://dx.doi.org/10.1364/AO.55.006559

1. INTRODUCTION

Lithium niobate ($LiNbO_3$) is among the most well known and widely used materials for nonlinear optics. The reasons for this widespread use are its large nonlinear coefficient, wide transparency range, commercial availability, and low cost [1].

Furthermore, $LiNbO_3$ has been studied extensively over the last several decades, resulting in both the implementation of quasi-phasematching (QPM) [2] as well as the development of several waveguide-fabrication technologies. Among the latter are methods based on the indiffusion of protons [3] or transition metals [4,5] to form the waveguide core, mechanically defined guiding structures via etching or dicing [6], or hybrid approaches [7]. The goal of these methods is to significantly increase the small-signal conversion efficiency of nonlinear frequency conversion by confining the interacting waves to a small cross section over an appreciable distance much greater than their natural diffraction length. Normalized conversion efficiencies for second-harmonic generation (SHG) at 1.55 μm (fundamental wavelength) exceeding 3%/mW can easily be achieved in congruently melting lithium niobate (CLN) [8]. This high normalized mixing efficiency, in combination with low propagation losses on the order of 0.1 dB/cm at 1.55 μm, makes such devices suitable for a wide range of applications requiring high conversion efficiencies at low input powers, such as optical signal processing [9], quantum optics [10], and pulse characterization [11].

The arguably easiest, fastest, cheapest, and most flexible way to form waveguides in lithium niobate is via proton exchange [3]. Here, lithium ions are being exchanged for hydrogen ions inside a hot acid bath. A number of acids have been successfully used as proton sources [12–14], with benzoic acid [3] being the most common one. Researchers have developed a large number of integrated structures using this ion-exchange technology, ranging from power splitters to mode converters and WDMs [9]. Since these structures are lithographically defined on a wafer scale, a large number of devices can be fabricated rapidly in a minimal number of steps.

While many of lithium niobate's material properties make it an ideal candidate for a growing number of applications in nonlinear optics, it is well known that it suffers from photorefractive damage (PRD) [15]. Light at visible and near-infrared wavelengths propagating through $LiNbO_3$ generates charge carriers that are trapped adjacent to the beam [16]. These trapped charges form a space-charge field, which, in combination with the electro-optic properties of the material, can cause severe wavefront distortion [17].

Mitigation approaches to limit the effects of PRD include increasing the material's photoconductivity, resulting in a reduction of the space-charge field and hence in the associated phase shifts. This reduction can be achieved, for example, by stoichiometry control, as in the case of stoichiometric lithium tantalate [18] and niobate [19], or by ion doping, as is done in 5% magnesium-oxide-doped lithium niobate (MgO:LN) [20]; there are other dopants, such as zinc [21], indium [22], and hafnium [23], which have been reported to reduce PRD.

Due to MgO:LN's commercial availability and PRD resistance, the application of the ion-exchange process would be desirable. Unfortunately, the diffused proton distribution in MgO:LN, and hence index profile, does not resemble the smooth high-peak-index profile obtained in CLN [24]. It has been shown that APE waveguides exhibit a conversion efficiency that is about three times lower than that in CLN due to low beam confinement and a suboptimal mode-overlap integral [25].

In this paper, we evaluate the proton-diffusion properties in zirconium-oxide-doped lithium niobate (ZrO:LN). This PRD-resistant material system is relatively new, with the first published work from Nankai University in 2007 [26–29]. Most of the previously reported work concentrated on the material's PRD properties as well as linear and nonlinear optical constants as a function of doping level [29]. It was shown that the "doping threshold" for PRD resistance, i.e., the minimum dopant concentration required to suppress PRD, lies somewhere between 2 and 3 mol. % of zirconium oxide inside the melt, resulting in a PRD threshold in excess of 160 kW/cm^2 at near-UV wavelengths (351 nm) [27]. Additionally, it has recently been demonstrated, by analyzing samples grown using the same crystal-growth process used for the samples analyzed here, that by doping with 3 mol. % of zirconium oxide, the photorefractive effect is strongly suppressed in the VIS and also in the NIR range [17]. It should also be noted that the distribution coefficient of ZrO_2 in $LiNbO_3$ is nearly unity, which should allow for the fabrication of large homogeneous boules. Additionally, the lower doping threshold compared to MgO:LN suggests that proton diffusion in ZrO:LN may have a more advantageous diffusion behavior.

2. SAMPLE PREPARATION

The starting material used in these experiments was obtained by slicing and polishing of a single-domain boule of ZrO:LN grown by the Czochralski process (3 mol. % zirconium oxide in the melt, see Ref. [28] for details). The homogeneity of the grown boules was controlled by evaluating the length of the lattice parameters, which are strongly dependent on the Zr content of the crystal [28], on samples taken from different parts of the boules. To determine whether proton diffusion in ZrO:LN can be approximated using a linear diffusion model, we created a set of four planar-waveguide samples by proton exchange to initial depths ranging from 0.92 to 1.98 μm in a bath of molten benzoic acid; an additional set of four CLN planar-waveguide samples were processed together with these ZrO:LN samples to serve as references.

To accurately determine the as-exchanged proton dose (exchange depth) for each of the samples, a series (264 h broken into 20 steps) of low-temperature anneals in air at 202°C were performed to reduce the crystalline phase mixture, resulting in a single-phase, step-like proton profile, which also proves to be stable over time [30]. This process has been called "soft anneal." This simple soft anneal has proven crucial for the development of the highly accurate proton-diffusion model for CLN [31]. The reason for its importance can be summarized as follows. An as-exchanged waveguide consists of a mixture of crystalline phases, whose composition depends on several parameters, such as acid age, temperature, and exchange depth. Such a multiphase film is unpredictable and even changes with time at room temperature. It is therefore a poor choice as an initial condition for a diffusion process.

The samples were characterized after each soft-anneal segment using a prism coupler (Metricon 2020) to determine the surface refractive index as well as layer thickness, assuming a step profile. It was determined that the extraordinary refractive index step of a fully soft-annealed ZrO:LN sample is 0.0985 at 632.8 nm and 0.1285 at 457.9 nm. For comparison, the corresponding values for CLN are 0.104 and 0.132, respectively. The uncertainty of the initial proton dose (exchange depth) was determined to be less than 1%.

These samples were subsequently annealed in air at 312°C for a total of 260 h, again divided into several steps. After each annealing segment, the effective indices of the waveguide modes were measured at both 623.8 and 457.9 nm using the prism coupler. From the effective indices of the modes, a continuous index profile was constructed using the well-known inverse-WKB (iWKB) method [32].

3. NONLINEAR DIFFUSION MODEL

The $1/e$ profile depth of all iWKB profiles for all samples normalized to their soft-anneal depth (d_{SA}) as a function of normalized anneal time ($\tau = t/d_{SA}^2$) is shown in Fig. 1; superposed is the prediction of a linear diffusion model showing that a nonlinear diffusion model is needed to explain the experimental results, as is also the case with undoped CLN. The evolution of the effective mode indices as a function of τ for one particular ZrO:LN sample is shown in Fig. 2. For comparison, the

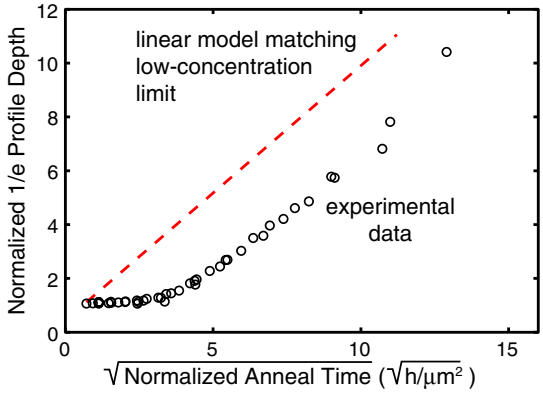

Fig. 1. Experimental data showing the normalized planar-waveguide depth versus normalized anneal time for protonated ZrO:LN. A linear diffusion model chosen to match the low-concentration (long-time) limit of the diffusion process, indicated by the dashed line, cannot be used to model proton diffusion in this material.

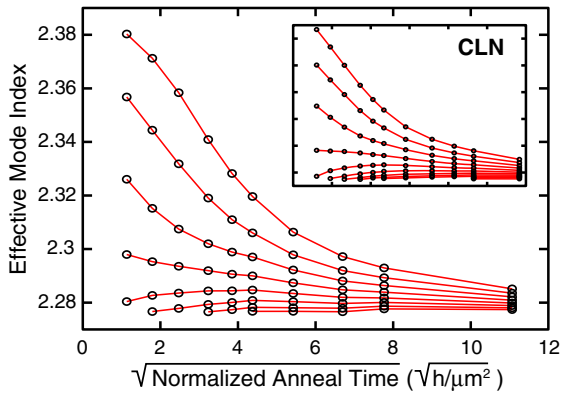

Fig. 2. Effective indices of guided modes in planar protonated ZrO:LN as a function of anneal time measured at 457.9 nm. Inset shows the corresponding results for protonated CLN for comparison. Connecting lines drawn to guide the eye.

corresponding plot for a CLN sample of comparable soft-anneal depth, shown in the inset, exhibits a striking resemblance.

Using a nondimensionalized nonlinear diffusion equation [Eq. (1)], a concentration profile was calculated and transformed into an index profile, making assumptions described below. These measured and simulated index profiles were compared and model parameters adjusted to achieve the best match.

$$\frac{dC'}{d\tau} = \frac{d}{dz'}\left\{D(C')\frac{dC'}{dz'}\right\}$$
$$C' = \frac{C}{C_{SA}} \quad \tau = \frac{t}{d_{SA}^2} \quad z' = \frac{z}{d_{SA}}. \tag{1}$$

For this analysis, a suitable expression for the nonlinear diffusion constant $D(C')$ must be chosen. For proton diffusion in CLN, several expressions were developed purely empirically [31,33], but publications describing single-phase proton exchange have shown that a $1/(C'+\alpha)$ dependence is to be expected for this process [34,35]. Roussev *et al.* [31] added an additional parameter to allow for the presence of higher-concentration phases. The expression used here is shown in Eq. (2) as follows:

$$D(C') = D_T\left\{\alpha + \frac{1-\alpha}{\beta C' + \gamma}\right\}, \tag{2}$$

with $[D_T] = \mu m^2/h$, and dimensionless parameters α, β and γ.

These parameters in the diffusion coefficient are obtained by fitting to empirical concentration profiles. Since we directly observe the refractive index profile rather than the concentration of protons, the relation between concentration and index change is required. Conversion between the simulated annealed proton profile and a refractive index profile requires knowledge of the material's refractive index as a function of concentration. Unfortunately, such a measurement is not trivial. The empirical approach followed here, as well as in previous work on CLN [31,33], is to assume the simplest possible relationship that can be supported by experimental measurements. For CLN, this dependence is linear. With respect to proton loss during annealing, while Korkishko observed a nontrivial loss of protons after long anneals at much higher temperatures than used in our studies [36], there is no evidence for proton loss at temperatures similar to those used in this study; for protonated CLN processed under similar conditions, no proton loss was observed [24]. The conserved proton number and a linear relation between the refractive index and the proton concentration together mean that the area under the index profile should be independent of the annealing time; changes in this area indicate violation of one of these assumptions.

Using a linear relationship between index change and proton concentration, we calculated the area underneath the iWKB profiles as a function of anneal time and noticed that the loss in area was much more pronounced for ZrO:LN than CLN (50% versus 30%). In the case of CLN, it appears that the loss in area is mainly due to the long, poorly resolved tail of the iWKB index profile, indistinguishable from the substrate refractive index, which results in significant numbers of protons that are not accounted for in the measured area of the index profile [24]. The next simpler model is a continuous piecewise-linear index model, with the boundary of the two linear segments parameterized by C_1 and dn_1 [see Fig. 3(a)]. Since we do not have a phase diagram for ZrO:LN at this moment, we placed the break point at the phase boundary of the α and κ phase at the same concentration as is observed in CLN and adjusted the index value while observing the loss-of-area plot, as shown in Fig. 3(b). The goal was to observe a constant area for the first couple of anneal steps while accepting a moderate loss for later anneals. This outcome would be consistent with our understanding of the effective-index measurement

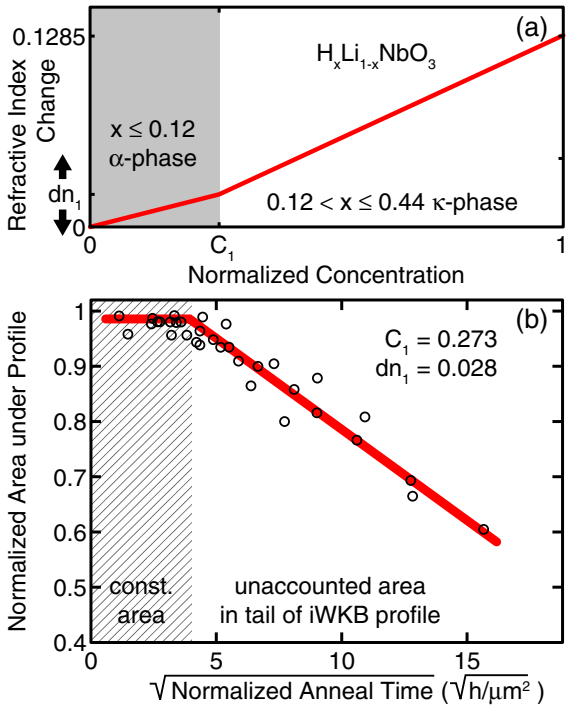

Fig. 3. (a) Continuous piecewise-linear index model resulting in a desired loss-of-area plot shown in (b) motivated by observations in protonated CLN. The model parameters are shown in (b) with the adjusted experimental values exhibiting a hockey-stick-like behavior (solid line).

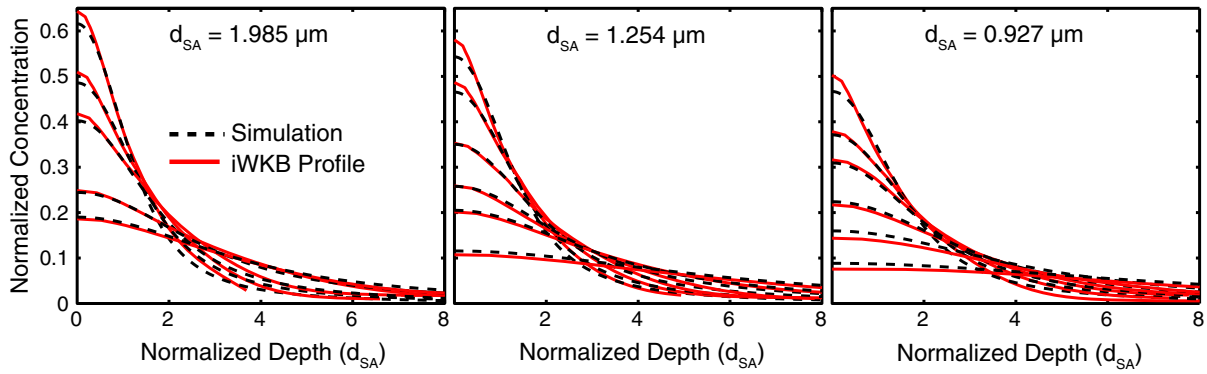

Fig. 4. Comparison between simulated concentration profiles (dashed lines) and iWKB profiles (solid lines) based on effective-index measurements at several stages of annealing (e.g., $\sqrt{\tau} \in [3.4, 8.2]\sqrt{\mathrm{h}/\mu\mathrm{m}^2}$ for the left-most sample). Good agreement can be observed for a large range of initial soft-anneal depths (d_{SA}) from 0.93 to 1.98 μm.

procedure and was achieved by choosing $C_1 = 0.273$ and $dn_1 = 0.028$.

Our currently best estimate for the diffusion parameters for ZrO:LN are

$$D_T = 14.67\ \mu\mathrm{m}^2/\mathrm{h}, \quad \alpha = 0.0015, \quad \beta = 1135, \quad \text{and} \quad \gamma = 0.4727,$$

with the simulation and iWKB profiles for three out of the four samples shown in Fig. 4. We notice that the match, while not as perfect as in the case of CLN, should be good enough to make accurate predictions about the device performance of practical APE waveguides in ZrO:LN. The current parameters cover a large range of soft-anneal depths from 0.93 to 1.98 μm.

4. CONCLUSION

In this paper, we have shown that ZrO:LN is a suitable material for the application of APE technology. Its favorable PRD properties, comparable to those of the widely used MgO:LN, make it a promising material for high-power nonlinear-optics applications, while its proton-diffusion properties resemble those of congruently melting lithium niobate, presenting an advantage compared to MgO:LN. It remains to be seen how much the presence of indiffused protons influences its damage resistance. The one-dimensional model that we have presented here is a first step toward the development of a two-dimensional diffusion model, as was done for CLN [24], required for the numerical simulation of channel waveguides. Furthermore, since buried waveguides exhibit increased modal overlaps and lower propagation losses, exploring reverse proton exchange [37] for this material presents an interesting future topic.

Funding. Air Force Office of Scientific Research (AFOSR) (FA9550-09-1-0233, FA9550-05-1-0180); Fondazione Ca. Ri.Pa. Ro (Excellence Project 2008-2009).

REFERENCES

1. P. F. Bordui and M. M. Fejer, "Inorganic crystals for nonlinear optical frequency conversion," Annu. Rev. Mater. Sci. **23**, 321–379 (1993).
2. S. Matsumoto, E. J. Lim, H. M. Hertz, and M. M. Fejer, "Quasiphase-matched second harmonic generation of blue light in electrically periodically-poled lithium tantalate waveguides," Electron. Lett. **27**, 2040–2042 (1991).
3. J. L. Jackel, C. E. Rice, and J. J. Veselka, "Proton exchange for high-index waveguides in $LiNbO_3$," Appl. Phys. Lett. **41**, 607–608 (1982).
4. G. P. Bava, I. Montrosset, W. Sohler, and H. Suche, "Numerical modeling of Ti:$LiNbO_3$ integrated optical parametric oscillators," IEEE J. Quantum Electron. QE/**23**, 42–51 (1987).
5. D.-L. Zhang, C.-X. Qiu, W.-J. Du, W.-H. Wong, and E. Y.-B. Pun, "$Zr4^+$/$Ti4^+$ codiffusion characteristics in lithium niobate," J. Am. Ceramic Soc. **98**, 567–573 (2015).
6. M. Asobe, H. Miyazawa, O. Tadanaga, Y. Nishida, and H. Suzuki, "A highly damage-resistant Zn:$LiNbO_3$ ridge waveguide and its application to a polarization-independent wavelength converter," IEEE J. Quantum Electron. **39**, 1327–1333 (2003).
7. J. Sun, Y. Gan, and C. Xu, "Efficient green-light generation by proton-exchanged periodically poled MgO:$LiNbO_3$ ridge waveguide," Opt. Lett. **36**, 549–551 (2011).
8. Z. Jiang, D. S. Seo, S. D. Yang, D. E. Leaird, R. V. Roussev, C. Langrock, M. M. Fejer, and A. M. Weiner, "Four-user, 2.5-Gb/s, spectrally coded OCDMA system demonstration using low-power nonlinear processing," J. Lightwave Technol. **23**, 143–158 (2005).
9. C. Langrock, S. Kumar, J. E. McGeehan, A. E. Willner, and M. M. Fejer, "All-optical signal processing using $\chi^{(2)}$ nonlinearities in guided-wave devices," J. Lightwave Technol. **24**, 2579–2592 (2006).
10. J. S. Pelc, L. Yu, K. D. Greve, P. L. McMahon, C. M. Natarajan, V. Esfandyarpour, S. Maier, C. Schneider, M. Kamp, S. Höfling, R. H. Hadfield, A. Forchel, Y. Yamamoto, and M. M. Fejer, "Downconversion quantum interface for a single quantum dot spin and 1550-nm single-photon channel," Opt. Express **20**, 27510–27519 (2012).
11. H. Miao, S.-D. Yang, C. Langrock, R. V. Roussev, M. M. Fejer, and A. M. Weiner, "Ultralow-power second-harmonic generation frequency-resolved optical gating using aperiodically poled lithium niobate waveguides," J. Opt. Soc. Am. B **25**, A41–A53 (2008).
12. K. Yamamoto and T. Taniuchi, "Characteristics of pyrophosphoric acid proton-exchanged waveguides in $LiNbO_3$," J. Appl. Phys. **70**, 6663–6668 (1991).
13. E. Pun, K. K. Loi, and P. S. Chung, "Proton-exchanged optical waveguides in z-cut $LiNbO_3$ using phosphoric acid," J. Lightwave Technol. **11**, 277–284 (1993).
14. Y. Korkishko, V. Fedorov, and O. Feoktistova, "$LiNbO_3$ optical waveguide fabrication by high-temperature proton exchange," J. Lightwave Technol. **18**, 562–568 (2000).
15. A. M. Glass, D. Linde, D. H. Auston, and T. J. Negran, "Excited state polarization, bulk photovoltaic effect and the photorefractive effect in electrically polarized media," J. Electron. Mater. **4**, 915–943 (1975).
16. H. Serreze and R. B. Goldner, "Study of the wavelength dependence of optically induced birefringence change in undoped $LiNbO_3$," Appl. Phys. Lett. **22**, 626–627 (1973).
17. G. Nava, P. Minzioni, I. Cristiani, N. Argiolas, M. Bazzan, M. V. Ciampolillo, G. Pozza, C. Sada, and V. Degiorgio, "Photorefractive

effect at 775 nm in doped lithium niobate crystals," Appl. Phys. Lett. **103**, 031904 (2013).
18. M. Katz, R. K. Route, D. S. Hum, K. R. Parameswaran, G. D. Miller, and M. M. Fejer, "Vapor-transport equilibrated near-stoichiometric lithium tantalite for frequency-conversion applications," Opt. Lett. **29**, 1775–1777 (2004).
19. F. Jermann, M. Simon, and E. Krätzig, "Photorefractive properties of congruent and stoichiometric lithium niobate at high light intensities," J. Opt. Soc. Am. B **12**, 2066–2070 (1995).
20. D. A. Bryan, R. Gerson, and H. E. Tomaschke, "Increased optical damage resistance in lithium niobate," Appl. Phys. Lett. **44**, 847–849 (1984).
21. Y. Zhang, Y. Xu, M. Li, and Y. Zhao, "Growth and properties of Zn doped lithium niobate crystal," J. Crystal Growth **233**, 537–540 (2001).
22. H. Qiao, J. Xu, C. Lou, G. Zhang, X. Zhang, Q. Wu, and G. Zhang, "The optical damage of indium doped lithium niobate crystals at UV," in *Photorefractive Effects, Materials, and Devices* (Optical Society of America, 2003), p. 106.
23. L. Razzari, P. Minzioni, I. Cristiani, V. Degiorgio, and E. P. Kokanyan, "Photorefractivity of hafnium-doped congruent lithium-niobate crystals," Appl. Phys. Lett. **86**, 131914 (2005).
24. R. V. Roussev, "Optical-frequency mixers in periodically poled lithium niobate: materials, modeling and characterization," Ph.D. thesis (Stanford University, 2006).
25. R. V. Roussev, V. Bhagavatula, J. Himmelreich, K. Becken, and J. Tingley, "Reverse-proton-exchanged waveguide frequency doublers for green light generation," Proc. SPIE **7917**, 79171Z (2011).
26. Y. Kong, S. Liu, Y. Zhao, H. Liu, S. Chen, and J. Xu, "Highly optical damage resistant crystal: zirconium-oxide-doped lithium niobate," Appl. Phys. Lett. **91**, 081908 (2007).
27. F. Liu, Y. Kong, W. Li, H. Liu, S. Liu, S. Chen, X. Zhang, R. Rupp, and J. Xu, "High resistance against ultraviolet photorefraction in zirconium-doped lithium niobate crystals," Opt. Lett. **35**, 10–12 (2010).
28. N. Argiolas, M. Bazzan, M. V. Ciampolillo, P. Pozzobon, C. Sada, L. Saoner, A. M. Zaltron, L. Bacci, P. Minzioni, G. Nava, J. Parravicini, W. Yan, I. Cristiani, and V. Degiorgio, "Structural and optical properties of zirconium doped lithium niobate crystals," J. Appl. Phys. **108**, 093508 (2010).
29. G. Nava, P. Minzioni, W. Yan, J. Parravicini, D. Grando, E. Musso, I. Cristiani, N. Argiolas, M. Bazzan, M. V. Ciampolillo, A. Zaltron, C. Sada, and V. Degiorgio, "Zirconium-doped lithium niobate: photorefractive and electro-optical properties as a function of dopant concentration," Opt. Mater. Express **1**, 270–277 (2011).
30. Y. N. Korkishko and V. A. Fedorov, "Relationship between refractive indices and hydrogen concentration in proton exchanged $LiNbO_3$ waveguides," J. Appl. Phys. **82**, 1010–1017 (1997).
31. R. Roussev, X. Xie, K. Parameswaran, M. Fejer, and J. Tian, "Accurate semi-empirical model for annealed proton exchanged waveguides in z-cut lithium niobate," in *IEEE LEOS Annual Meeting Conference* (IEEE, 2003), Vol. **1**, pp. 338–339.
32. K. S. Chiang, "Construction of refractive-index profiles of planar dielectric waveguides from the distribution of effective indexes," J. Lightwave Technol. **3**, 385–391 (1985).
33. M. L. Bortz and M. M. Fejer, "Annealed proton-exchanged $LiNbO_3$ waveguides," Opt. Lett. **16**, 1844–1846 (1991).
34. T. Veng and T. Skettrup, "Ion exchange model for α phase proton exchange waveguides in $LiNbO_3$," J. Lightwave Technol **16**, 646–649 (1998).
35. Y. N. Korkishko, V. A. Fedorov, E. A. Baranov, M. V. Proyaeva, T. V. Morozova, F. Caccavale, F. Segato, C. Sada, and S. M. Kostritskii, "Characterization of α-phase soft proton-exchanged $LiNbO_3$ optical waveguides," J. Opt. Soc. Am. A **18**, 1186–1191 (2001).
36. Y. N. Korkishko, V. A. Fedorov, O. Y. Feoktistova, and T. V. Morozova, "Effect of SiO_2 cladding on properties of annealed proton-exchanged $LiNbO_3$ waveguides," J. Appl. Phys. **87**, 4404–4409 (2000).
37. K. R. Parameswaran, R. K. Route, J. R. Kurz, R. V. Roussev, M. M. Fejer, and M. Fujimura, "Highly efficient second-harmonic generation in buried waveguides formed by annealed and reverse proton exchange in periodically poled lithium niobate," Opt. Lett. **27**, 179–181 (2002).